Karlsruher Institut für Technologie

Numerical studies on oxygen-assisted methane conversion under compression-expansion conditions

Master thesis from

Georgios Iosifidis

Karlsruhe Institute of Technology

Institute of Technical Thermodynamics

First reviewer:	Prof. Dr. rer. nat. habil. Ulrich Maas
Second reviewer:	Dr.-Ing. Robert Schießl
Supervisor:	Dr.-Ing. Robert Schießl

01.12.2021-01.06.2022

Declaration of originality

I hereby declare that I have composed this paper by myself and without any assistance other than the sources given in my list of works cited. This paper has not been submitted in the past or is currently being submitted to any other examination institution. It has not been published. All direct quotes as well as indirect quotes which in phrasing or original idea have been taken from a different text (written or otherwise) have been marked as such clearly and in each single instance under a precise specification of the source. I am aware that any false claim made here results in failing the examination.

Date: 01.06.2022 Signature:

Acknowledgments

I would like to especially thank my mother and father for supporting me all these years throughout my studies. It would not have been possible to pursue engineering without their continuous support and encouragement.

I express my sincere gratitude to my supervisor Dr.-Ing. Robert Schießl who patiently assisted me with every problem I encountered while working on this thesis and - with his lectures - shaped my interest in the area of technical thermodynamics.

Last but not least, I must thank my brother, who stood by me in times of difficulty from the very beginning and helped me become a better person. I owe him a lot.

Abstract

The production of chemical energy carriers using renewable energy can be an essential component of the future energy system. One particular application of this concept is the use of piston engines to convert methane into valuable species like acetylene (C_2H_2), hydrogen (H_2), and ethylene (C_2H_4). The conversion process is called pyrolysis and often demands very high-temperature levels to be carried out (800–1200 °C) [1]. Prior research has shown that a high argon dilution is necessary to achieve those high temperatures in a piston engine [2]. However, it is because of this that the mass fraction of the products is relatively low. In order to avoid this strong argon dependence, oxygen-assisted conversion in a motor piston engine is studied in this thesis—combustion results in high temperatures, which probably can lead to the desired conversion. The piston engine is modeled as a compression-expansion cycle with detailed chemical kinetics in this study. The mixture's initial composition, which enters the engine, consists of oxygen, argon, and methane, and the target quantities are methane conversion and products' yield and mass fraction. It turns out that methane can be 100% converted, and good yields for acetylene (70%), hydrogen (90%), and ethylene (30%) can be achieved for the initial temperature of 400K.

Table of contents

1. Introduction

1.1 Motivation

Energy conversion systems have always been in the research spotlight because of their various advantages. Over the centuries, many devices and systems have been developed, while today, the research seems to turn towards renewable energy sources (solar, wind, hydropower, etc.)

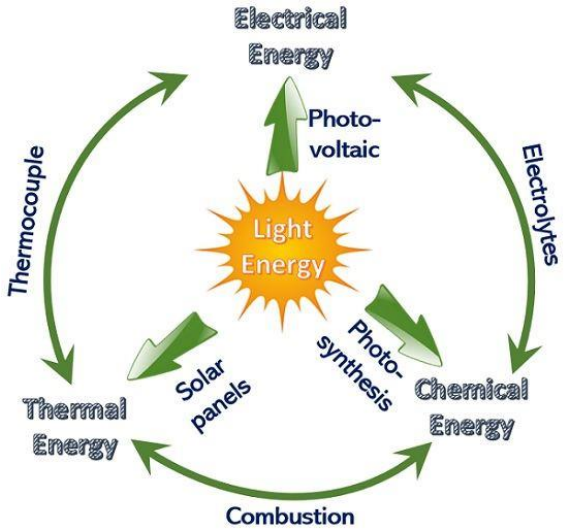

Picture 1.1: Energy conversion cycle
https://beingintelligent.com/energy-conversion.html

Picture 1.1 depicts the energy transformation cycle, including different ways to convert energy from one form to another.

However, further research for new and innovative energy conversion systems should be carried out to find systems that can convert widespread energy sources into something valuable. A related energy conversion concept is being studied systematically in this thesis. Nowadays, because of the excess mechanical energy in today's industrialized society, it would be beneficial to find various ways to exploit work. The idea described in this thesis is flexible energy conversion from mechanical to chemical energy using methane (CH_4), a cheap and widely available substance. Engines running in homogeneous charge compression ignition (HCCI) mode can be used in pyrolysis operations, where high temperatures at the top dead center (TDC) following compression induce endothermal reactions. In order to boost the temperatures and promote the conversion, the mixture is also diluted with argon and oxygen. Argon is an inert gas and does not take part in any reaction. What it does instead

is to help raise the temperature inside the cylinder since it has a low specific heat capacity (Cp). Oxygen can also contribute to temperature rise with both its lower heat capacity than methane and its reactivity. During the compression stroke, mechanical energy (work) is converted to thermal energy due to exothermal reactions. Then, thermal energy is converted to chemical energy due to endothermal reactions.

1.2 State of the art

Piston engines offer the ability for high pressure and temperature conditions for a limited time. Thus, many scientists have considered them as potential chemical reactors, where reactions are initiated by compression heating and subsequently quenched by gas expansion. Many previous works have investigated polygeneration reactors that can contribute to both chemical energy storage and chemical synthesis. In 1956, Von Szeszich L. produced syngas in a spark-ignition (SI) engine through partial oxidation of methane/oxygen mixtures [3]. This section summarizes in bullets some of the scientific papers regarding the most recent research on flexible energy conversion from mechanical to chemical energy:

- A motored piston engine with a high but realistic compression ratio and engine speed (22:1, 3000 RPM) at inlet temperatures between 323 and 573 K, pressures between 1 and 10 bar, and argon dilution between 85 and 99 mol% were used to study the pyrolysis of methane and ethane from a chemical energy storage perspective. According to the results, at 573 K (methane) and 473 K (ethane), a conversion of above 80% is predicted for an argon dilution of 93 mol%. An efficiency of 75% (methane) and 70% (ethane) is predicted for a 400 ccm four-stroke single-cylinder with a storage capacity of 7.5 kW and 6 kW, respectively [4].

- The initial composition consisted of methane, argon, and helium has been tested in a Rapid Compression Machine (RCM) to produce unsaturated hydrocarbons (C_2H_2, C_2H_4) and hydrogen. It has been shown that by increasing temperature, the yields of H_2, C_2H_2, and C_2H_4 increase but the yield of C_2H_4 reaches a saturation. Moreover, the conversion turns out to be almost independent of pressure. The highest conversion was found for a mixture of 1 mol-% CH_4 and 99 mol-% of noble gas (Ar + He) [5].

- Furthermore, pulsed compression in a pulsed compression reactor (PCR) has opened up a new possibility for converting methane under non-oxidative and non-catalytic conditions into ethylene with promising conversion and selectivity. Without hydrogen in the feed, the attainable operating window (C2-selectivity vs. methane conversion) observed was similar to other catalytic oxidative and non-oxidative coupling processes. With hydrogen, 24% C_2-yield (62% ethylene selectivity, 93% C_2-selectivity) at 26% methane conversion was reached without observable soot [6].

- Last but not least, a fuel-rich conversion of methane as a fuel has been investigated both experimentally and numerically, with different literature oxidation mechanisms for fuel-rich mixtures (from $\phi = 2$ to ∞). With an engine running in HCCI mode, methane converts to synthesis gas with work and heat output at equivalence ratios below 2. Better yields of higher hydrocarbons are achieved at higher equivalence ratios, where although the soot formation is stronger. Based on that idea, recirculation of hot exhaust gases has also been studied. Energy efficiencies up to 80% were achieved, leading to reduced fuel consumption with up to 40% fuel savings when compared to separate production of power, heat, and hydrogen [7].

1.3 Problem Statement

This work studies the potential of using a motor piston engine as a reactor for chemical conversion. The main objective is to study oxygen-assisted methane conversion for production of unsaturated hydrocarbons (C_2H_2, C_2H_4, CO) and hydrogen.

2. Methodology

The topic of the research is studied numerically. For that reason, both modeling and simulations are part of the Methodology.

2.1 Model

The gas mixture is subjected to compression-expansion with a prescribed volume curve. Temperature, pressure, volume, and possibly chemical conversion change under the influence of that volume curve. In the first part of the Model, the process's volume profile is described and follows the thermodynamic and chemical kinetic parts.

2.1.1 Volume Profile

The chosen volume curve is a trigonometric function of time, according to the following mathematical expression: $V_{cyl}(t) = a + b \cdot cos(\omega t)$, where t is for time, ω for the crank angular velocity and a, b are parameters. To define a, b and ω, engine speed (N), compression ratio (CR) and maximum volume (V_{max}) are selected. Specifically, the resulting system of equations is the following:

$$V_{cyl}(t) = a + b \cdot cos(\omega t) \tag{2.1.1}$$

$$CR = \frac{V_{max}}{V_{min}} = 20 \tag{2.1.2}$$

$$V_{max} = a + b = 0.5lt \tag{2.1.3}$$

$$V_{min} = a - b \tag{2.1.4}$$

$$N = 1000rpm \tag{2.1.5}$$

$$\omega = \frac{2\pi N}{60} \tag{2.1.6}$$

The solution of the system of equations (2.1.1) ∧ (2.1.2) ∧ (2.1.3) ∧ (2.1.4) ∧ (2.1.5) ∧ (2.1.6) gives the following mathematical expression that will be used for the majority of the simulations:

$$V_{cyl}(t) = 0.2625 + 0.2375cos\ (104.67t) \qquad (2.1.7)$$

with $t[=]s$ and $V_{cyl}[=]lt$

The graphical depiction of the volume profile with time is presented in figure 2.1

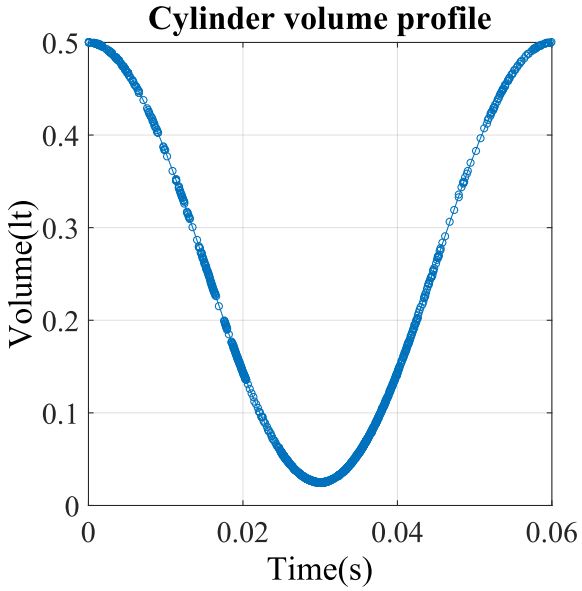

Figure 2.1: Cylinder volume profile with equal timed compression and expansion of 0.03s

2.1.2 Thermodynamic Assumptions

For the simplification of the thermodynamic state description of the mixture, the following assumptions are made:

- All the gases are considered to be ideal.
- The piston work is performed reversibly.
- The mixture is homogenous, which means that the gas mixture has the same properties at every point.

- During the compression-expansion process, there are no mass losses.

- The piston moves fast enough, so there are no heat losses during the process.

2.1.3 Thermodynamic Equations

A state vector is defined to describe the state variables at each time t:

$$\boldsymbol{Y}(t) = \begin{pmatrix} P \\ V \\ T \\ N_1 \\ . \\ . \\ . \\ N_{n_s} \end{pmatrix} \tag{2.1.3.1}$$

Here P denotes the pressure, V the volume, T the temperature, and N_i the moles with $i = \{1, \ldots, n_s\}$ the index for the number of different species.

In the following, the basic thermodynamic equations and principles are shown, with the help of which one can calculate the time evolution of $\boldsymbol{Y}(t)$ can be calculated:

- The differential form of 1st law of thermodynamics in a closed system with the time derivative of the internal energy $\dot{U}$, work $\dot{W}$ and the convective heat transfer $\dot{Q}$:

$$\dot{U} = \dot{W} + \dot{Q} \tag{2.1.3.2}$$

- The time derivative of the reversibly performed piston work:

$$\dot{W} = -P\dot{V} \tag{2.1.3.3}$$

- The ideal gas law:

$$P \cdot V = N_i R_u T \tag{2.1.3.4}$$

where R_u is the universal gas constant and equal to $8.3145\ \frac{J}{mol\ K}$

- The internal energy of a mixture of gases can be expressed as:

$$U = \sum_{i=1}^{n_s} N_i \cdot \overline{U}_i \tag{2.1.3.5}$$

where $\overline{U}_i$ denotes the molar internal energy of species i.

- Differentiating both sides of equation (2.1.3.5) yields:

$$\dot{U} = \sum_{i=1}^{n_s} \dot{N}_i \cdot \overline{U}_i + \sum_{i=1}^{n_s} N_i \cdot \dot{\overline{U}}_i \tag{2.1.3.6}$$

- The change in molar internal energy of species i is given by the following equation:

$$\overline{U}_i = \bar{C}_{v,i} \cdot \dot{T} \tag{2.1.3.7}$$

- Chemical source term:

$$\omega_i = \left(\frac{\partial c_i}{\partial t}\right)_{chem} = \sum_{r=1}^{R} k \cdot \left(v_{ri}^{(p)} - v_{ri}^{(e)}\right) \prod_{s=1}^{S} c_s^{v_{rs}^{(e)}} \tag{2.1.3.8}$$

This equation expresses the rate of change in concentration of a species as a function of stoichiometric coefficients of reactants. *R* is the number of reactions and S the number of species. The stoichiometric coefficients of reactants and products are given by $v_{ri}^{(p)}$ and $v_{ri}^{(e)}$ respectively. The concentration of the s element is denoted by c_s while k is the rate coefficient of the reaction.

2.1.4 Chemical Kinetics

Chemical kinetics provides practical information about the time scale the reactions occur, comparable with the flow and molecular transport processes [8]. In this section, essential reactions and laws will be discussed to be able to explain the results in the following Chapter.

To begin with, the difference between elementary and net reactions (or overall reactions) is a fundamental point. An elementary reaction is one that occurs on a molecular level exactly in the way which is described by the reaction equation. On the other hand, overall reactions are reactions that are a consequence of many elementary reactions. The reactions that are in the spotlight of this study are the following:

$CH_{4(g)}+2O_{2(g)}\rightarrow CO_{2(g)}+2H_2O(g)$ $\quad \Delta h^o_{298K} = -802.3\ \frac{kJ}{mol}$ (2.1.4.1)

$CH_{4(g)}+0.5O_{2(g)}\rightarrow CO(g)+2H_2(g)$ $\quad \Delta h^o_{298K} = -35.56\ \frac{kJ}{mol}$ (2.1.4.2)

$CH_{4(g)}\rightleftarrows C_2H_2(g)+H_2(g)$ $\quad \Delta h^o_{298K} = 376.4\ \frac{kJ}{mol}$ (2.1.4.3)

$CH_{4(g)}\rightleftarrows 0.5C_2H_4(g)+H_2(g)$ $\quad \Delta h^o_{298K} = 201.9\ \frac{kJ}{mol}$ (2.1.4.4)

Reactions (2.1.4.1), (2.1.4.2), (2.1.4.3) and (2.1.4.4) are overall reactions.

It has been observed that the rate coefficient k of the chemical reactions depends strongly and in a nonlinear way on the temperature. According to Arrhenius (1889), this is the formula that describes their relationship:

$$k = A' \cdot e^{\frac{-E_a}{RT}} \tag{2.1.4.5}$$

where A' is the pre-exponential factor that shows temperature dependence according to the following formula $A' = AT^b$ with $-1 < b < 1$. E_a is the reaction's activation energy, i.e., the energy barrier that has to be overcome for the reaction to start.

Under previous research, the activation energy for the thermal dissociation of methane ranges from 312 to 450 $\frac{kJ}{mol}$, whereas preexponential factors between $8.46 \cdot 10^9\ \frac{1}{s}$ and $2.8 \cdot 10^{16}\ \frac{1}{s}$ [9].

Another source mentions an Arrhenius coefficient of $8.3 \cdot 10^{11}\ \frac{cm^3}{mol \cdot s}$ and activation energy of $30000\ \frac{cal}{mol}$ for the overall combustion reaction of methane [10].

2.2 Simulations

This part of the Methodology is dedicated to the simulations of the thesis. Mainly, it refers to the solution of the differential equations system and the programs that have been used to solve it numerically. Last but not least, reference is made to the concept of the simulations.

2.2.1 Solution

Due to $ns + 3$ variables in the state vector $\boldsymbol{Y}(t)$, a system of differential equations with $ns + 3$ equations is necessary to solve this system:

$$\dot{\boldsymbol{Y}}(t) = f(t, \boldsymbol{Y}) \text{ with } \boldsymbol{Y}(0) = \boldsymbol{Y}_0$$

where $\boldsymbol{Y}_0$is the initial state vector of the system.

$$\boldsymbol{Y_0} = \begin{pmatrix} 0.25bar \\ V_{cyl}(0) \\ 400K \\ N_{CH4,0} \\ N_{Ar,0} \\ N_{O2,0} \end{pmatrix}$$

where $N_{CH4,0}$, $N_{Ar,0}$, $N_{O2,0}$ will be varied in the simulations

In particular, these are the ordinary differential equations that are used to solve the system:

- The time derivative of volume curve is the following:

$$\dot{V} = \dot{V}_{cyl}(t) \qquad (2.2.2.1)$$

- The time derivative of the amount of species in moles is obtained by the following computation:

$$\dot{N}_i = \omega_i \cdot V \qquad (2.2.2.2)$$

- Substituting the equations (2.1.3.3), (2.1.3.6) and (2.1.3.7) into the equation of the 1st law of Thermodynamics (2.1.3.2) yields to the time derivative of temperature:

$$\dot{T} = \frac{-P \cdot \dot{V} - \sum_{i=1}^{n_s} \dot{N}_i \cdot \bar{U}_i + \dot{Q}}{\sum_{i=1}^{n_s} \bar{C}_{v,i} \cdot N_i} \qquad (2.2.2.3)$$

- The time derivative of pressure results from the differentiation of the ideal gas equation (2.1.3.4):

$$\dot{P} = P \cdot \left(\frac{\sum_{i=1}^{n_s} \dot{N}_i}{\sum_{i=1}^{n_s} N_i} + \frac{\dot{T}}{T} - \frac{\dot{V}}{V} \right) \qquad (2.2.2.4)$$

The program used to solve the differential equations is called "HOMREA" (HOMogeneous REActor) and can compute time-dependent homogeneous reaction systems given the reaction mechanism [11]. The reaction mechanism used in this thesis is called "UCBChen49_20bar" and includes 49 species. It is a detailed reaction mechanism, valid for peak pressures close to 20bar, and shows good agreement with Rapid Compression Machine (RCM) experiments [12]. The simulation outputs are thermodynamic data such as temperature, pressure, mole fractions of the species, concentrations of the species, etc. Both the inputs and the outputs of the simulations have been controlled through MATLAB.

2.2.2 Concept of Simulations

The simulations are divided into two main parts. At the beginning, the aim is to study oxygen's physical and chemical effect and their mutual interaction as well, that can lead to methane conversion. In the second part follows a parametric study which includes the variation of the initial amount of oxygen, argon and methane, in order to understand the dependence of the target quantities (methane conversion, products' yield, and mass fraction) from the initial mixture composition ($CH_4/O_2/Ar$). Then, the suitable initial composition can be found, which results in the maximum amount of each target product (C_2H_2, C_2H_4, CO, H_2) at the end of the process.

The initial conditions of temperature, pressure, volume and compression ratio are constant and equal to 400K, 0.25bar, 0.5lt and 20, respectively. However, there are a few simulations to which exceptionally different than those conditions have been applied in order to show something very specific.

2.3 Definition of Quantities

In this part are being listed all the quantities that have been used for the description of the chemical species.

- Mole N_i:

$$N_i = \frac{m_i}{M_i} \tag{2.3.1}$$

where m_i and M_i denotes the mass and molar mass of species i, respectively

- Mole fraction x_i:

$$x_i = \frac{N_i}{\sum_{i=1}^{n_s} N_i} \tag{2.3.2}$$

where $N_t = \sum_{i=1}^{n_s} N_i$ is the total moles of the mixture.

- Mass fraction w_i:

$$w_i = \frac{m_i}{\sum_{i=1}^{n_s} m_i} \tag{2.3.3}$$

where m_i denotes the mass of species i and $m_t = \sum_{i=1}^{n_s} m_i$ denotes the total mass of the mixture. Furthermore, submitting equation (2.13) and (2.14) into equation (2.15) results to the following equation:

$$w_i = x_i \cdot \frac{M_i}{\sum_{i=1}^{n_s} N_i \cdot M_i} \tag{2.3.4}$$

where $M_t = \sum_{i=1}^{n_s} N_i \cdot M_i$ is the molar mass of the mixture.

- Yield y_p:

$$y_p = \frac{N_p - N_{p,0}}{N_{e,0}} \cdot \frac{\nu_p}{\nu_e} \tag{2.3.5}$$

where the indices e and p describe the educt or the product and the index 0 describes the inlet state. The parameter ν is the number of C and H atoms of the species to be calculated. The yields of hydrocarbons are referred to the C-atoms and the yield of the hydrogen is referred to the H-atoms.

- Methane conversion c_{CH_4}:

$$c_{CH_4} = \frac{N_{CH_4,i} - N_{CH_4,f}}{N_{CH_4,i}} \tag{2.3.6}$$

where $N_{CH_4,i}$ and $N_{CH_4,f}$ are the moles of methane in the inlet and final state, respectively.

- Equivalence ratio φ:

$$\varphi = \frac{(O/F)_{stoic}}{(O/F)_{act}} \tag{2.3.7}$$

where $(O/F)_{act}$ and $(O/F)_{stoic}$ indicate the actual and the stoichiometric oxidizer-fuel ratio based on mass, respectively

.

3. Results and Discussion

3.1 Physical and chemical effect of oxygen addition

3.1.1 Physical effect of oxygen addition

The physical effect of oxygen refers to oxygen's thermodynamic impact based on its heat capacity value. In order to isolate the physical effect from the chemical one, simulations with the reaction mechanism deactivated have been carried out. That means that the chemical source term is equal to zero ($\omega_i = 0$).

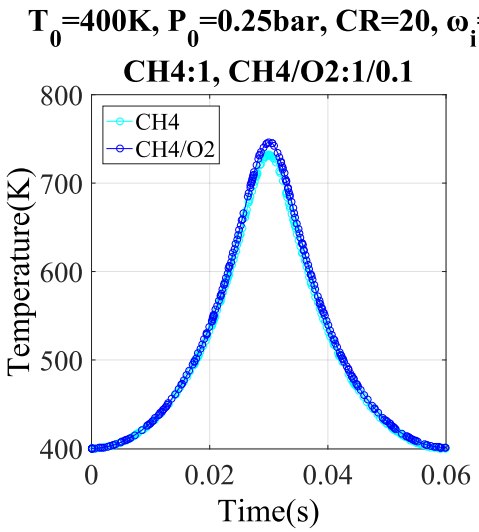

Figure 3.1: Comparison of time-temperature profiles of pure methane and mixture CH4/O2, with zero chemical source term, proving the temperature superiority of the last one

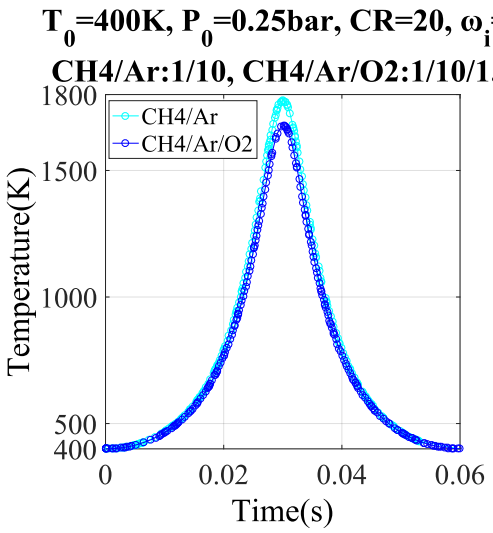

Figure 3.2: Comparison of time-temperature profiles of mixtures CH4/Ar and CH4/Ar/O2, with zero chemical source term, proving the temperature superiority of the first one

Figures 3.1 and 3.2 show the physical effect of oxygen when added to pure methane and CH_4/Ar mixture. Both mixtures CH_4/O_2 and $CH_4/Ar/O_2$ contain the same amount of oxygen ($x_{in,O2} = 9.1\%$). In figure 3.1, oxygen is added to pure methane, and as a result, the temperature decreases close to Top Dead Center (TDC). On the other hand, in figure 3.2, oxygen is added to CH_4/Ar mixture, and a temperature rise is caused. This contrast is due to argon's lower heat capacity than methane and oxygen.

Based on the difference in the temperature curves and since the gas mixtures are ideal ($Cp = Cp(T)$), it yields the following close to TDC:

$$Cp_{CH4/Ar} < Cp_{CH4/Ar/O2} < Cp_{CH4/O2} < Cp_{CH4}$$

3.1.2 Chemical effect of oxygen addition

An isochoric and adiabatic system has been simulated to observe the chemical effect of oxygen. Figure 3.3 shows the time-temperature profile of mixtures CH4/Ar and CH4/Ar/O2. The information about the chemical effect of oxygen lies behind the slope of the curves, which represents the time derivative of temperature $\dot{T} = \frac{\partial T}{\partial t}$. In addition, the conditions are suitable so that the reactions in both mixtures start (T_0=1700K, P_0=20bar).

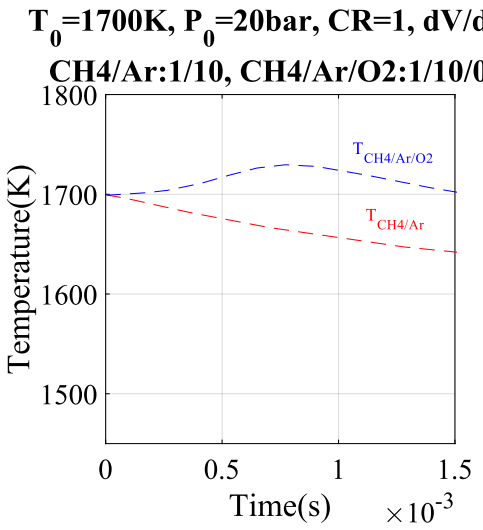

Figure 3.3: Comparison of time-temperature profiles of mixtures CH4/Ar and CH4/Ar/O2 in isochoric system

Adapting equation (2.2.2.3), yields $\dot{T} = \frac{-\sum_{i=1}^{n_s} \dot{N}_i \cdot \bar{U}_i}{\sum_{i=1}^{n_s} \bar{C}_{v,i} \cdot N_i}$. According to figure 3.4, for mixture CH4/Ar/O2, the first milliseconds apply $\dot{T} > 0$, while for mixture CH4/Ar applies $\dot{T} < 0$. The difference in the sign is due to the chemical effect of oxygen. Oxygen can run exothermal reactions, which lead to temperature increase. On the other hand, in mixture CH4/Ar, there are only endothermal reactions running, and that's why the temperature immediately decreases. Furthermore, oxygen reacts very fast, which makes it a very good temperature booster for the endothermal reactions

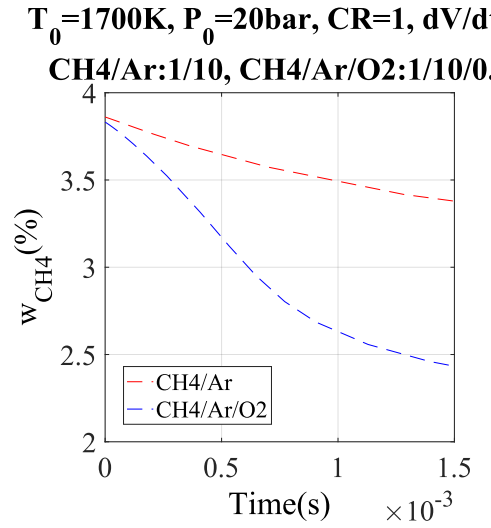

Figure 3.4: Time-methane mass fraction profile of mixtures CH4/Ar and CH4/Ar/O2 in isochoric system

In figure 3.4, the slope of the curves represents the time derivative of methane mass fraction $\dot{w} = \frac{\partial w}{\partial t}$. The curve of the mixture with oxygen is steeper than the one without: $|\dot{w}_{no\ O2}| < |\dot{w}_{with\ O2}|$. That result can be explained by the Arrhenius equation (2.1.4.5), according to which, a temperature boost leads to increase of the reaction rate. Based on that principle, there is an excellent potential for methane conversion enhancement with oxygen, since it can stimulate exothermal reactions.

3.1.3 Physical and chemical effect combined

After the study of both effects separately, it is worth investigating their mutual interaction. In that case compression-expansion conditions are applied with reaction mechanism in active mode.

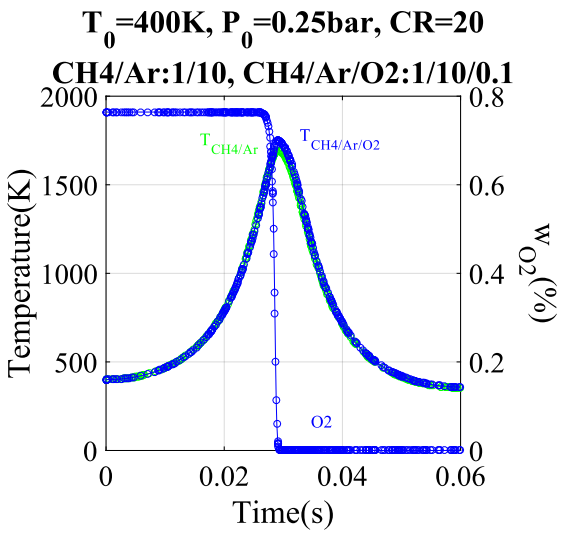

Figure 3.5: Temperature superiority of mixture CH4/Ar/O2 over CH4/Ar because of oxygen's combined physical and chemical effect

In figure 3.5, the time-temperature profiles of mixtures CH4/Ar and CH4/Ar/O2 and time-mass fraction profile of oxygen of the second mixture are depicted. The temperature difference is not so easily distinguishable in that figure, because the oxygen initial mole fraction is not that high ($x_{in,O2} = 0.9\%$). However, the temperature superiority of mixture with oxygen over the one without, is clear. A zoom in close to TDC could give more information about the interaction.

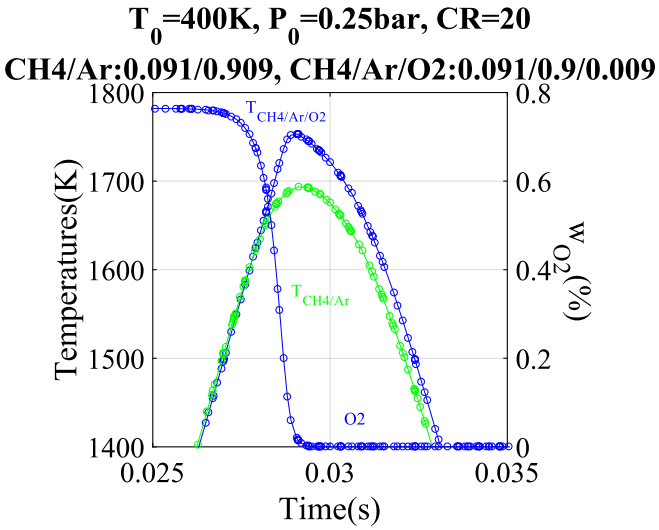

Figure 3.6: Zoomed figure 3.5, showing the combined physical and chemical effect of oxygen

In figure 3.6, in the beginning, both temperature curves are almost identical, which means the influence of argon is more dominant. Slightly before TDC, the curves stand out with the highest belonging to the mixture with oxygen. The advance of that curve is logical since oxidation has already started, as the oxygen profile shows. As a result, the temperature in mixture CH4/Ar/O2 is higher than that of mixture CH4/Ar.

From one point and after, though, the temperature difference between the two mixtures gets smaller as time goes by. That point is even closer to TDC and happens when the oxygen mass fraction in mixture CH4/Ar/O2 is almost zero. The reason is simply that the reactivity of oxygen leads to oxygen consumption, so when oxygen's amount gets to zero, the mixture does not have its temperature enhancement anymore.

Therefore, even though oxygen leads to temperature decrease only due to its physical effect, it contributes overall to the compression temperature rise. According to the Arrhenius equation (2.1.4.5), temperature impacts methane conversion, as the following figure shows.

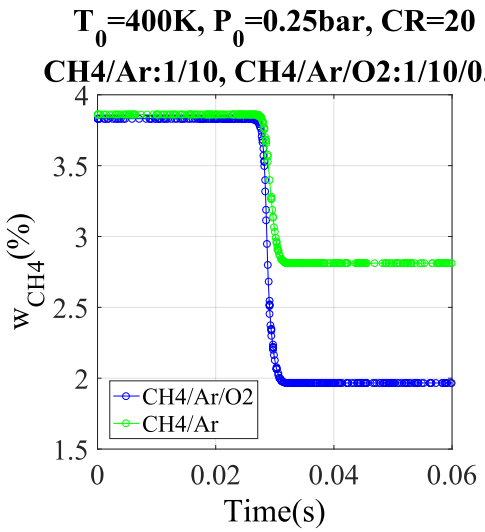

Figure 3.7: Time-methane mass fraction profiles of mixtures CH4/Ar/O2 and CH4/Ar that show the methane conversion enhancement due to oxygen

In accordance with figure 3.8, oxygen addition offers a greater methane conversion under compression-expansion conditions, and that is because of the temperature's superiority of mixture CH4/Ar/O2 over mixture CH4/Ar.

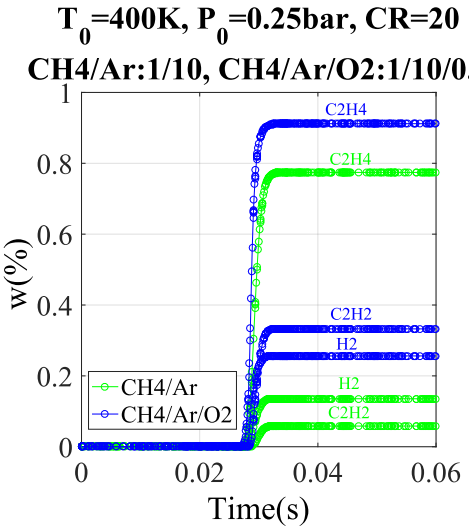

Figure 3.8: Mass fraction profiles of the target species of mixtures CH4/Ar/O2 and CH4/Ar with time

In figure 3.8, the time-mass fraction profiles of the target species are being compared. Based on the diagram, the amounts of acetylene, ethylene, and hydrogen at the end of the process reach higher values when oxygen is added to the initial mixture.

3.2 Parametric studies

According to the chemical and physical properties of oxygen and some raw data in the previous subchapter, oxygen addition in the initial mixture is a promising way to improve methane conversion. What incites the interest now is how initial composition affects the target quantities of the target species (C_2H_2, C_2H_4, H_2, CO) at the end of the process. The parametric studies are divided into two parts regarding the degree of freedom of the system. Subchapter 3.2.1 is dedicated to one degree of freedom system, and subchapter 3.2.2 to two degrees of freedom system.

3.2.1 One degree of freedom

In this section, the initial mole fraction of oxygen and φ are varied, while the mole ratio $\frac{x_{in,Ar}}{x_{in,CH4}}$ is constant and equal to 10. Considering also that always applies $x_{in,CH4} + x_{in,Ar} + x_{in,O2} = 1$, the system is of one degree of freedom. Figures 3.9 and 3.10 present the dependence of the target quantities on oxygen's initial mole fraction and φ respectively. The left y-axe is for the yield and the right y-axe is for the methane conversion percentage.

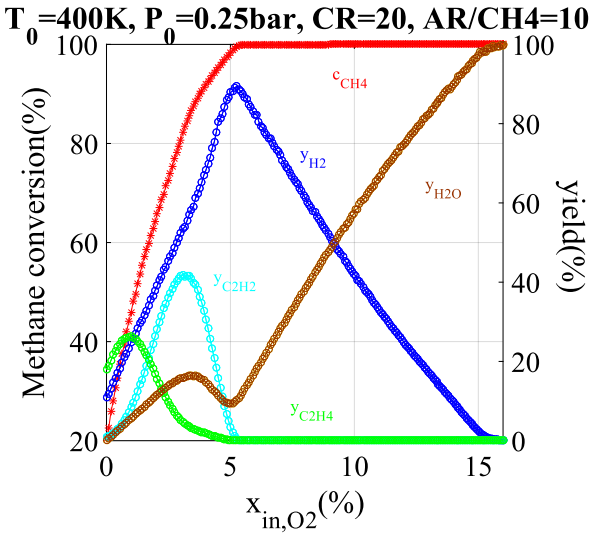

Figure 3.9: Methane conversion and target species yield dependence on the initial mole fraction of oxygen

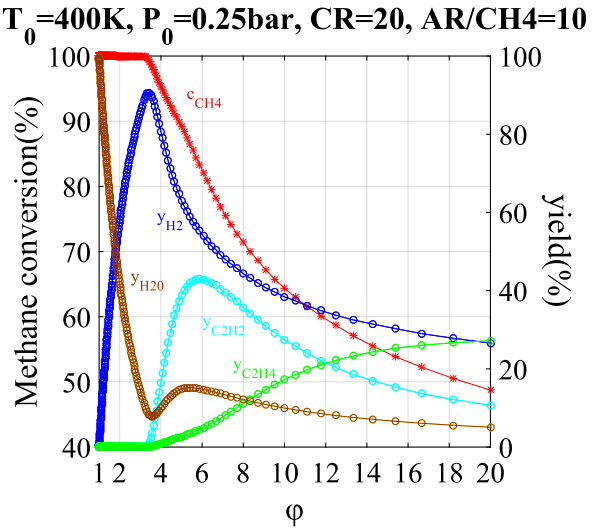

Figure 3.10: Methane conversion and target species yield dependence on φ

The two diagrams look similar, and that is because of the relationship between the initial mole fraction of oxygen and φ. Equation (2.3.7) implies $\varphi = \frac{2x_{in,CH4}}{x_{in,O2}}$, which means that φ and initial mole fraction of oxygen are inversely proportional. That is why figure 3.10 looks like figure 3.9 but inversed.

The starting values of yield and methane conversion represent the case of no oxygen inlet ($\varphi = Inf$), meaning methane pyrolysis. As the amount of oxygen inlet increases, more methane is being converted. That happens because more oxygen leads to combustion even closer to the complete one. Thus, even less methane remains after oxidation to be decomposed. From around 5% initial mole fraction of oxygen ($\varphi = 3.3$) and after, the amount of methane available after partial oxidation is being totally decomposed. By increasing further the initial amount of oxygen, even more methane is being partially oxidized until complete combustion is reached ($\varphi = 1$).

From $\varphi = 20$ to $\varphi = 3.3$, the hydrogen yield increases and moving from $\varphi = 3.3$ to $\varphi = 1$ decreases. The explanation behind that phenomenon is that in the first area incomplete combustion (reaction 2.1.4.2) is more dominant and in the second one, complete combustion (reaction 2.1.4.1) starts to be more dominant until the condition $\varphi = 1$ is reached. That claim can be verified by the fact that water formation is low at the beginning and then starts to increase as complete combustion is being approached. From $\varphi = 3.3$ and after, the sum of the yields of hydrogen and water are equal to 100%. That indicates that the only compound that takes the molecule of hydrogen away in that area is water. For $\varphi = 1.8$, the yield of hydrogen and water are both equal to 50%.

Except for yield, mass fraction profiles are also worthy of investigation. They give direct information about the actual results at the end of the process, and they offer a quantitative view of the target species. Figures 3.11 and 3.12 reflect their mass fraction profiles regarding the initial mole fraction of oxygen and φ, respectively.

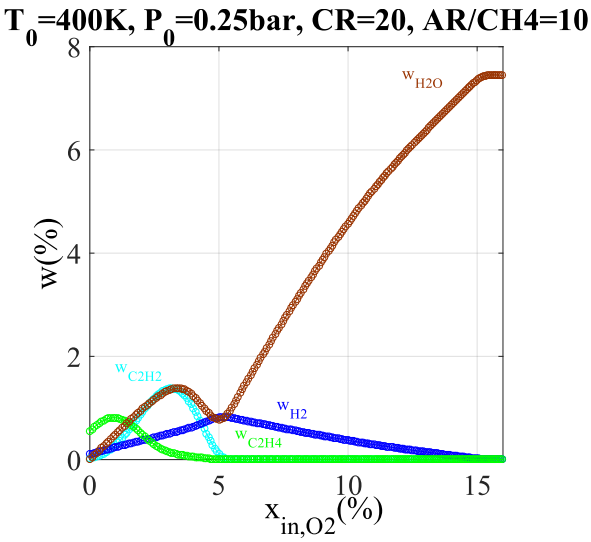

Figure 3.11: Target species mass fraction dependence on the initial mole fraction of oxygen

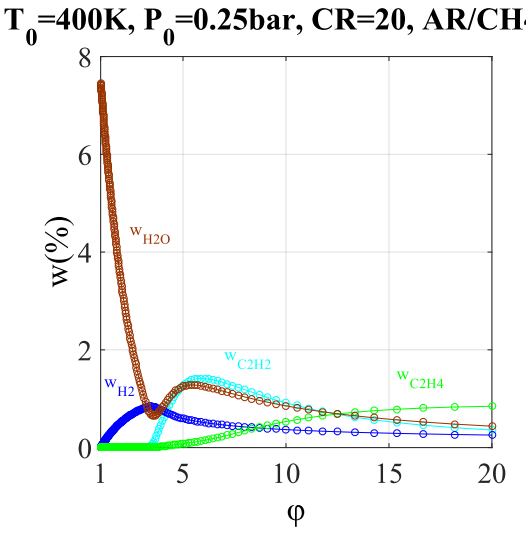

Figure 3.12: Target species mass fraction dependence on φ

Figures 3.10 and 3.11 show that all the mass fraction of acetylene, ethylene, and hydrogen doesn't go over 2%, which is probably due to the various products that resulting from oxidation, such as water and carbon monoxide. Furthermore, the mass fraction of acetylene increases for a greater amount of oxygen than ethylene does. The reason is that acetylene is more stable than ethylene in high temperatures. Last but not least, the maximum values in yields of every depicted species appear at the same positions where the corresponding mass fractions maxima appear, since the mole ratio $\frac{x_{in,Ar}}{x_{in,CH4}}$ is constant during the simulations.

3.2.2 Two degrees of freedom

To gain a more spherical view of the process, the last part of chapter 3 is dedicated to the variation of the initial mass fraction of argon and the new variable called φ*. This new term is similar to φ and aims to include in the simulations the case for $\varphi = Inf$. Specifically, $\varphi^* = \frac{\varphi}{1+\varphi}$ and $\varphi = Inf$ implies $\varphi^* = 1$ and $\varphi = 1$ implies $\varphi^* = 0.5$.

For all the following simulations, a 31x31 mesh has been created. Argon initial mass fraction ranges from 80 to 100%, while φ^* from 0.5 to 1. The interesting area is after $\varphi^* = 0.5$ because, for lower values, there is lean combustion.

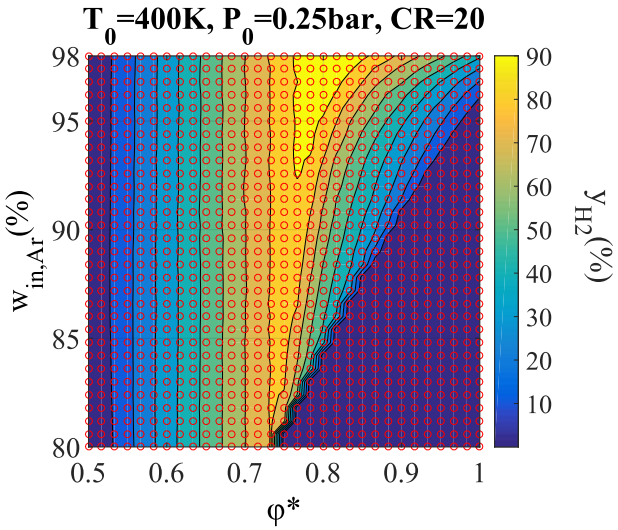

Figure 3.13: Hydrogen yield dependence on φ* and the initial mass fraction of argon

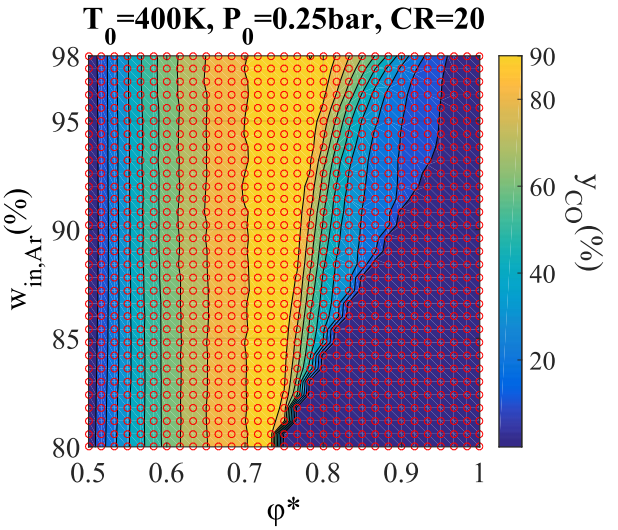

Figure 3.14: Carbon monoxide yield dependence on φ* and the initial mass fraction of argon

In figures 3.13 and 3.14, hydrogen and carbon monoxide dependence on argon and $\varphi^*$is depicted, respectively. In both figures, there are parallel contour areas from $\varphi^* = 0.5$ to 0.75. That indicates that for a specific φ* value, any change in the initial argon mass fraction does not affect hydrogen and carbon monoxide yield, which means that argon has no significant influence on the temperature development for those φ* values. Moving horizontally leads to greater yield change than moving vertically, which shows that for $\varphi^* = 0.5$ to 0.75^* , methane/oxygen ratio plays a more decisive role in the temperature development than argon dilution.

Starting from the left ($\varphi^* = 0.5$), where there is complete combustion (reaction 2.1.4.1) and zero hydrogen and carbon monoxide production, and moving to the right, incomplete combustion (reaction 2.1.4.2) is getting more dominant. That can be verified by the fact that the yield of hydrogen and carbon monoxide increases. However, there is a turning point around $\varphi^* = 0.75$, after which the yield of both species decreases due to oxygen reduction, and more argon dilution is needed to achieve a higher yield. After that point there are no more parallel contour areas which means that argon dilution starts to play a more important role in the temperature development.

In the case of no oxygen ($\varphi^* = 1$), carbon monoxide yield is zero, while hydrogen yield ranges from $10\% - 30\%$, depending on the argon percentage.

Of great interest is the "deep blue triangle" on the downright side of figure 3.13. Something similar also appears on the downright side of figure 3.14. That indicates that no hydrogen and carbon monoxide is produced at the end of the process because oxygen is not enough, and methane is left after the process.

According to both figures, the maximum yield of both species is 90%. However, in the case of carbon monoxide, it is being achieved for a wider range of argon initial mass fraction values.

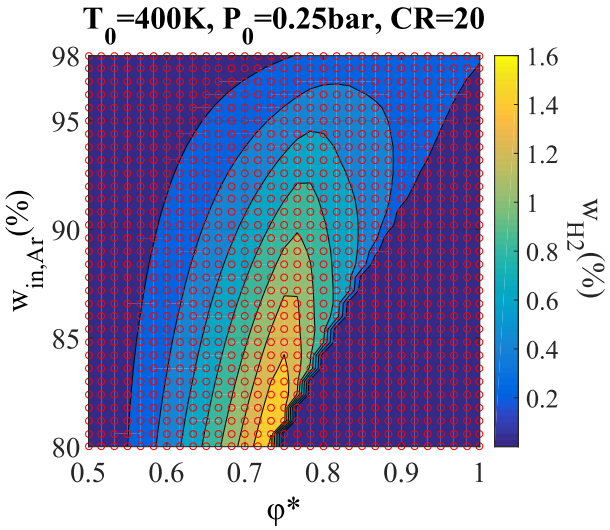

Figure 3.15: Hydrogen mass fraction dependence on φ* and the initial mass fraction of argon

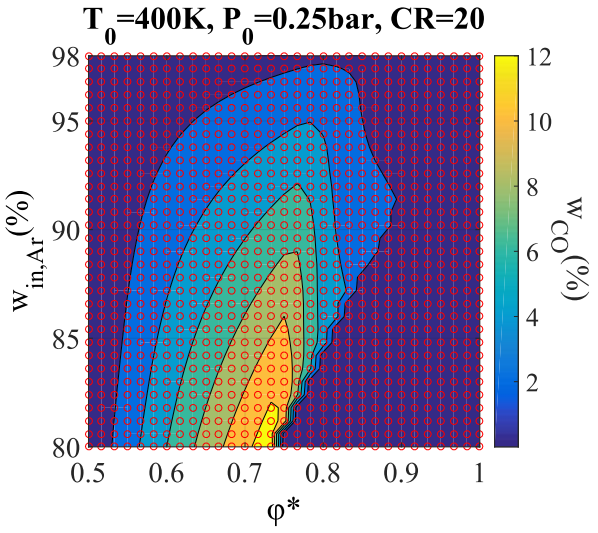

Figure 3..16: Carbon monoxide mass fraction dependence on φ* and the initial mass fraction of argon

It is easily noticeable that mass fractions diagrams differ significantly from the yield ones, with the most remarkable difference being the maxima positions. However, that can be explained by the fact that high argon initial mass fraction leads a priori to low hydrogen and carbon monoxide rates. Since argon does not participate in the reactions, its high percentage initially remains high also at the end.

The colored area in both figures is surrounded by deep blue areas, which correspond to zero mass fraction of hydrogen and carbon monoxide. Analytically, the blue area left to the colored one is due to few methane that is left after oxidation and no hydrogen or carbon monoxides is being produced. On the other hand, the deep blue area right the colored one is because of the low amount of oxygen, resulting much methane remaining.

The maximum mass fraction of hydrogen is 1.6% and is achieved for φ^* values between 0.71 and 0.75 and argon initial mass fraction between 80% and 84%. Without oxygen addition ($\varphi^* = 1$), there is no significant hydrogen production (0.2%). On the other hand, the maximum mass fraction of carbon monoxide is 12% and is achieved for φ^* values between 0.71 and 0.73 and argon initial mass fraction between 80% and 82%.

Generally, both diagrams look similar schematically because hydrogen's production is also ruled by the same oxidation reaction as carbon monoxide's (reaction 2.1.4.2).

As far as the hydrocarbons is concerned, figure 3.17 and 3.18 show acetylene and ethylene yield diagrams, respectively.

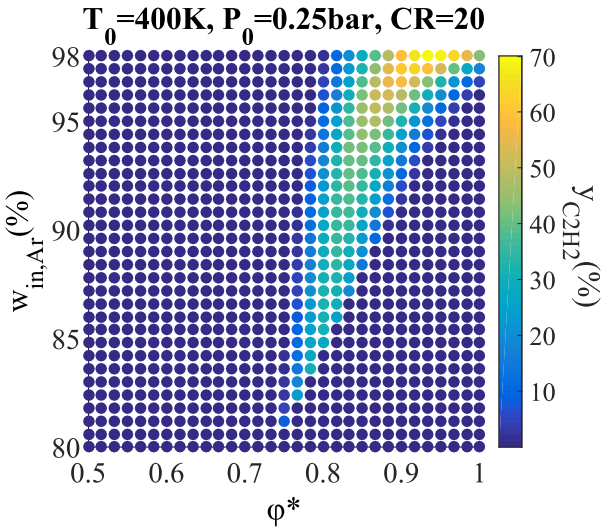

Figure 3.17: Acetylene yield dependence on φ^* and the initial mass fraction of argon

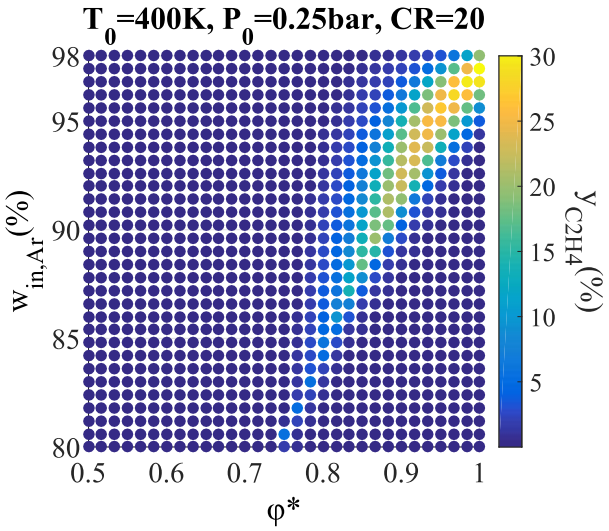

Figure 3.18: Ethylene yield dependence on φ^* and the initial mass fraction of argon

In contrast with hydrogen's yield figure, for φ^* values lower than 0.75, there are zero yields for both acetylene and ethylene. The reason is that hydrogen is a product not only of methane decomposition but of methane oxidation too. Instead, in the case of the two hydrocarbons, they come only from methane decomposition.

Acetylene maximum yield is 70%, and ethylene's is 30%. A markable notice is that the maximum yield of ethylene appears for zero oxygen addition, but acetylene's for φ^* values between 0.92 and 0.94, meaning for a small amount of oxygen compared to methane. In both cases, though, a high percentage of argon is needed.

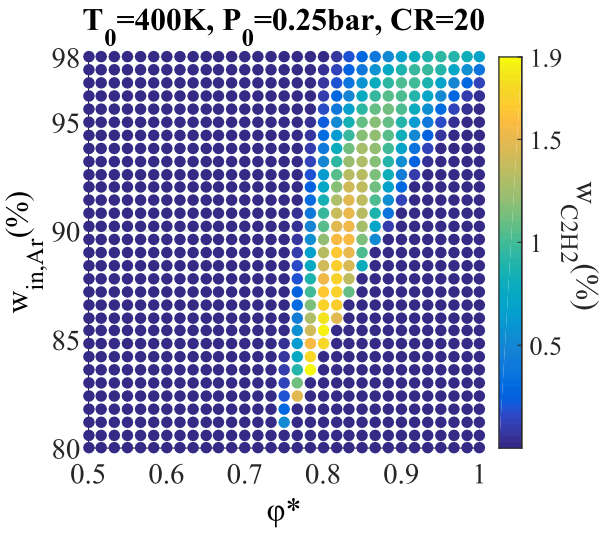

Figure 3.19: Acetylene mass fraction dependence on φ^* and the initial mass fraction of argon

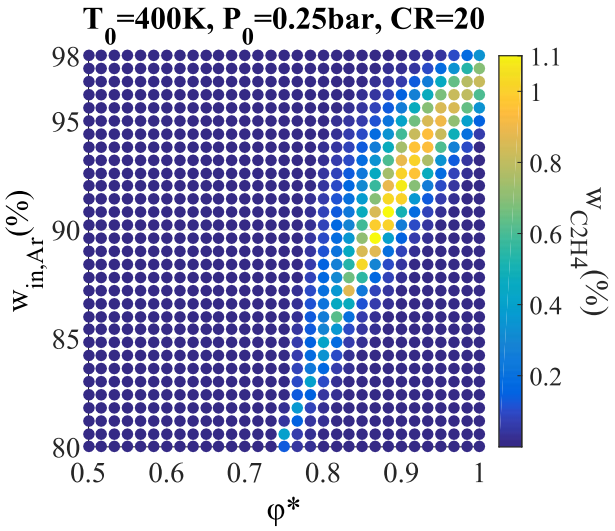

Figure 3.20: Ethylene mass fraction dependence on φ^* and the initial mass fraction of argon

Figures 3.19 and 3.20 present the corresponding plots of acetylene and ethylene mass fractions. Acetylene maximum mass fraction is 1.9% and is achieved for φ^* around 0.8 and around 85% initial mass fraction of argon. On the other hand, ethylene maximum mass fraction is 1.1% and is achieved for φ^* around 0.9 and around 90% initial mass fraction of argon.

Based on both mass fraction and yield diagrams of acetylene, ethylene, hydrogen, and carbon monoxide, there is a very sharp transition to the “deep blue triangle”. From

having a non-zero mass fraction/yield for the species, a step more to the right horizontally leads to zero production. This abrupt transition is perhaps due to the change of mixture's Cp. In fact, what is happening probably is that Cp increases moving horizontally and as a result the compression temperature decreases.

In order to prove that statement, simulations with increased initial temperature have been carried out. Figures 3.21 and 3.22 depict hydrogen yield and mass fraction at the end of the process with an initial temperature of 440K. The rest of the initial conditions are the same as in figures 3.13 and figure 3.15.

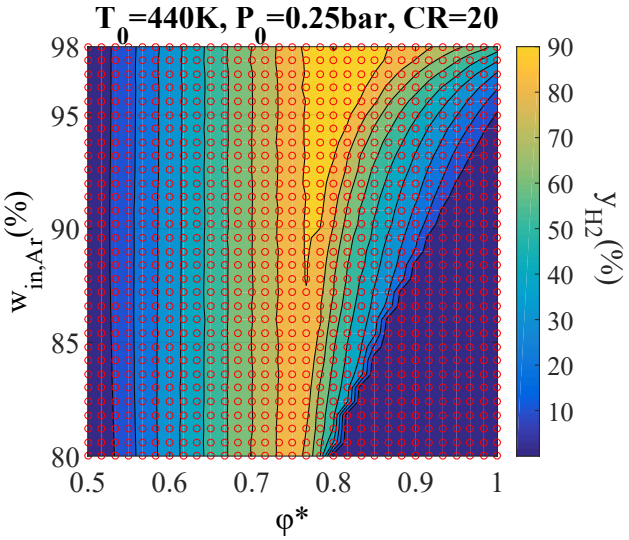

Figure 3.21: Hydrogen yield dependence on φ* and the initial mass fraction of argon for T_0=440K

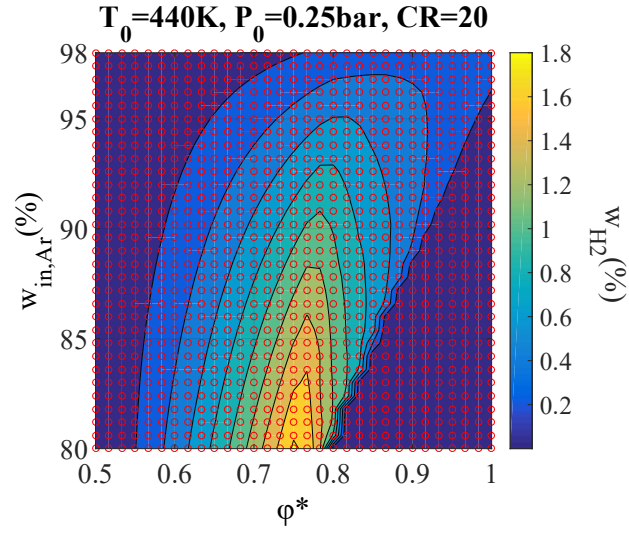

Figure 3.22: Hydrogen mass fraction dependence on φ* and the initial mass fraction of argon for T_0=440K

Comparing figure 3.13 to 3.21 and figure 3.15 to 3.22 yields a temperature dependence of that sharp limit. Analytically, that diagonal border of the triangle has been transferred more to the right in both mass fraction and yield figure when the initial temperature increased. Hence, for T_0=400K, the compression temperature is not high enough to stimulate oxygen's exothermal reactions. That means that the oxygen-assisted temperature boost strategy does not work anymore when that border is crossed.

When T_0=440K is applied, the maximum value of hydrogen mass fraction has been increased to 1,8% at the end of the process. In the case of hydrogen yield, the maximum area has been expanded to a lower initial mass fraction of argon.

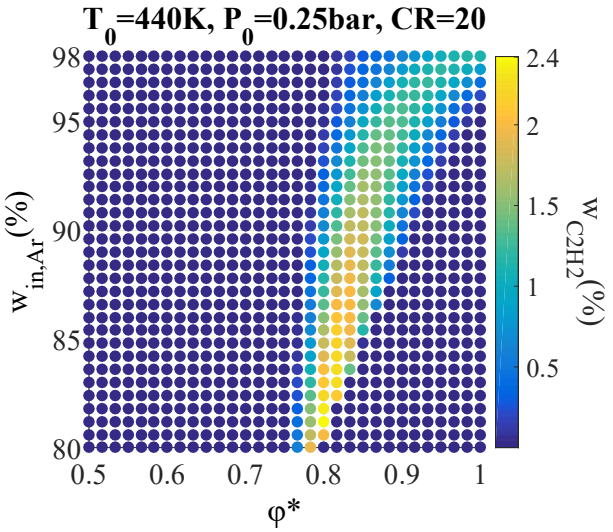

Figure 3.23: Acetylene mass fraction dependence on φ^* and the initial mass fraction of argon for T_0=440K

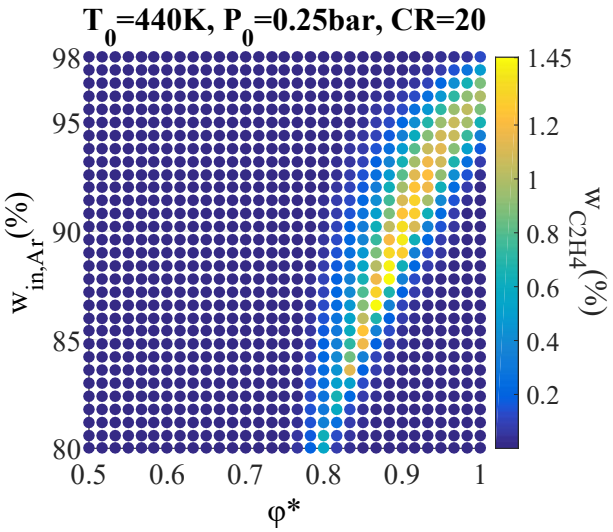

Figure 3.24: Ethylene mass fraction dependence on φ^* and the initial mass fraction of argon for T_0=440K

Figures 3.23 and 3.24 depict hydrogen yield and mass fraction at the end of the process with an initial temperature of 440K.

Comparing figure 3.23 to 3.19 and figure 3.24 to 3.20 yields that there is a mass fraction enhancement for both hydrocarbons and that the diagonal border of the “deep blue triangle” has also been transferred to the right. Analytically, with an 10% increase of the initial temperature, the mass fraction of acetylene increased by 26.32% and amount of ethylene by 31.82%.

4. Summary

In this master thesis, the influence of oxygen on methane conversion under the isentropic compression-expansion process has been numerically investigated. It was found that oxygen can lower the activation energy of the endothermal reactions and enhance the production of both unsaturated hydrocarbons and hydrogen. The following are the most representative findings that are derived from this thesis:

- Complete methane conversion can be achieved even with a small initial amount of oxygen (5%), argon initial mole fraction below 90% (86.2%), and equivalence ratio equal to 3.3.

- The maximum yields for C_2H_2, C_2H_4, and H_2 are 70%, 30%, and 90%, respectively.

- Oxygen-assisted methane conversion can lead to higher mass fractions for the target species (C_2H_2, C_2H_4, H_2) than methane pyrolysis.

- The final mass fraction of the target species (C_2H_2, C_2H_4, H_2) does not exceed 2%. In contrast with CO, which can go above 10%.

To sum up, this oxygen-assisted method looks very promising regarding methane conversion under compression-expansion conditions. It offers encouraging results, especially for hydrogen production. Furthermore, oxygen-assisted conversion paves the way for the reduction of argon amount needed since argon can be partly replaced as a temperature booster by the exothermal reactions of oxygen.

Last but not least, research on other initial conditions and volume curves is recommended for future work to optimize the process. In the context of this thesis, there was a quick allusion to slight preheating, which shows that in combination with the appropriate oxygen amount, it can lead to further independence from argon and better results. Moreover, experiments would also be useful to verify the numerical results.

List of Figures

List of Pictures

References

[1] Guéret, C.; Michel Daroux, M.; Billaud, F., "Methane pyrolysis: thermodynamics", *Chemical Engineering Science*, vol. 52, 1997, pp. 815-827., https://doi.org/009-2509/97 $17.00 + 0.00

[2] Atakan, B., "Compression–Expansion Processes for Chemical Energy Storage: Thermodynamic Optimization for Methane, Ethane and Hydrogen.", *Energies*, vol. 12, 2019, pp. 1-21., https://doi.org/10.3390/en12173332

[3] Von Szeszich, L., "Herstellung von Synthesegas im Otto-Motor bei gleichzeitiger Arbeitsgewinnung", *Chemie Ingenieur Technik*, vol. 28, 1956, pp.190-195, https://doi.org/10.1002/cite.330280310

[4] Charlotte, R.; Atakan, B., "Pyrolysis of Methane and Ethane in a Compression–Expansion Process as a New Concept for Chemical Energy Storage: A Kinetic and Exergetic Investigation", *Energy Techology*, vol. 9, 2021, pp. 1-16, https://doi.org/10.1002/ente.202000948

[5] Drost, S.; Schießl, R.; Maas, U.; " Rapid Compression Machine (RCM) studies on the production of unsaturated hydrocarbons from methane", *Lecture held at 27th International Colloquium on the Dynamics of Explosions and Reactive Systems (ICDERS 2019),* Peking, China, 28. Juli–2. August 2019

[6] Slotboom, Y.; Roosjen, S.; Kronberg, A.; Glushenkov, M.; Kersten, S.R.A.; "Methane to ethylene by pulsed compression", *Chemical Engineering Journal*, vol. 414, 2021, pp. 1-7, https://doi.org/10.1016/j.cej.2021.128821

[7] Hegner, R.; Atakan, B., "A polygeneration process concept for HCCI-engines – Modeling product gas purification and exergy losses", *International Journal of Hydrogen Energy*, vol. 42, 2017, pp. 1-7, https://doi.org/10.1016/j.ijhydene.2016.09.050

[8] Warnatz, J.; Maas, U.; Dibble R.W., *Combustion: Physical and Chemical Fundamentals, Modeling and Simulation, Experiments, Pollutants Formation*, Springer, 2001

[9] Wullenkord M., *Determination of Kinetic Parameters of the Thermal Dissociation of Methane PhD Thesis*, 2011, German Aerospace Center in Cologne, Germany

[10] Rouband, A.; Mahulkar, V.; Leyland, P.; Favrat, D., In-cylinder combustion modeling with simplified chemistry, *14th Int. Multidimensional Engine Modeling User's Group Meeting*, 2003, USA

[11] Warnatz, J.; Maas, U., *Grundlagen Technischer Verbrennungsvorgänge*, Springer, Heidelberg (1993), Verbrennung, 2. Auflage (1996), 3. Auflage (2001)

[12] Drost, S.; Aznar, M.S.; Schießl, R.; Ebert, M.; Chen, J.; Maas, U., "Reduced reaction mechanism for natural gas combustion in novel power cycles", *Combustion and Flame*, vol. 223, 2021, pp. 1-9, https://doi.org/10.1016/j.combustflame.2020.09.029